Bioorganic & Medicinal Chemistry Letters 29 (2019) 1727–1731

Contents lists available at ScienceDirect

Bioorganic & Medicinal Chemistry Letters

journal homepage: www.elsevier.com/locate/bmcl

Utilizing comprehensive and mini-kinome panels to optimize the selectivity of quinoline inhibitors for cyclin G associated kinase (GAK)

Christopher R.M. Asquith[a,b,*], Daniel K. Treiber[c], William J. Zuercher[b,d,*]

[a] Department of Pharmacology, School of Medicine, University of North Carolina at Chapel Hill, Chapel Hill, NC 27599, USA
[b] Structural Genomics Consortium, UNC Eshelman School of Pharmacy, University of North Carolina at Chapel Hill, Chapel Hill, NC, 27599, USA
[c] Eurofins DiscoverX, 42501 Albrae Street, Fremont, CA 94538, USA
[d] Lineberger Comprehensive Cancer Center, University of North Carolina at Chapel Hill, Chapel Hill, NC 27599, USA

ARTICLE INFO

Keywords:
Cyclin G associated kinase (GAK)
4-anilinoquinoline
4-Anilinoquinazoline
Kinome selectivity
Mini-kinome panel

ABSTRACT

We demonstrate an innovative approach for optimization of kinase inhibitor potency and selectivity utilising kinase mini-panels and kinome-wide panels. We present a focused case study on development of a selective inhibitor of cyclin G associated kinase (GAK) using the quin(az)oline inhibitor chemotype. These results exemplify a versatile, efficient approach to drive kinome selectivity during inhibitor development programs.

A key challenge in developing kinase inhibitors that target the conserved ATP-binding site is inhibitor selectivity. The optimal screening approach would be to generate full kinome profiles for every compound prepared and thus provide a complete picture of compound selectivity.[1] Profiling every compound throughout a medicinal chemistry program is a costly and time-consuming endeavour. There is a need to economise to have the optimal balance of time, cost, and information for compound progression. This in practice means testing a subset of kinases against a subset of compounds at an early stage. Indeed, there is increasing data suggesting that focused, rationally-designed kinome mini panels can provide useful, representative data for wider kinome selectivity to effectively support discovery efforts.[2,3] Herein we exemplify this approach by applying it to an inhibitor series targeting cyclin G associated kinase (GAK).

The quin(az)oline is a common kinase inhibitor chemotype. Several quin(az)oline-based clinical kinase inhibitors show cross reactivity with GAK, including the approved drugs gefitinib, erlotinib, and bosutinib (Fig. 1).[4] These drugs were designed as inhibitors of either epidermal growth factor receptor (EGFR) or SRC family kinases and show similar or higher affinity for several other kinases, making them ineffective tools for direct interrogation of GAK biology.[5]

Isothiazolo[5,4-*b*]pyridine (JMC 2015-12g) was reported as a selective GAK inhibitor.[6] Although useful as a tool compound, JMC 2015-12g shows cross reactivity with other kinases, any of which may lead to confounding cell biology. The availability of a selective GAK chemical probe with a negative control would be a valuable asset for deconvoluting phenotypes associated with GAK.

GAK is a 160 kDa serine/threonine kinase originally identified as a direct association partner of cyclin G and a member of the numb-associated kinase (NAK) family.[7] In addition to its kinase domain, the GAK C-terminus has high homology with auxilin and tensin, with broad expression and localization to the Golgi complex, cytoplasm, and nucleus.[8,9]

GAK has been implicated in diverse biological processes, and genome-wide association studies have identified single nucleotide polymorphisms in the GAK gene associated with susceptibility to Parkinson's disease.[10] GAK is also involved in membrane trafficking and uncoating of clathrin-coated vesicles in the cytoplasm.[11,12] GAK is also required for maintenance of centrosome maturation and progression through mitosis.[13] GAK is over-expressed in osteosarcoma. In prostate cancer, GAK expression increases with the progression to androgen independence.[14–16] GAK inhibition may be associated with clinical toxicity due to pulmonary alveolar dysfunction. However, this speculation is based upon the phenotype of transgenic mice expressing catalytically inactive GAK and has not yet been tested with a selective small molecule GAK inhibitor.[17]

We are focused on elucidating the biology of GAK and other members of the lesser-studied portion of the kinome.[18] We have previously described the identification of a series of 4-anilinoquinoline inhibitors of GAK, exemplified by GW494610, GI230329 and **1**.[19] Quinoline **1** was profiled at 1 μM across an assay panel of over 400 wild-type human kinases (KINOMEscan). Subsequent K_D determination

* Corresponding authors.
E-mail addresses: chris.asquith@unc.edu (C.R.M. Asquith), william.zuercher@unc.edu (W.J. Zuercher).

https://doi.org/10.1016/j.bmcl.2019.05.025
Received 4 March 2019; Received in revised form 14 May 2019; Accepted 15 May 2019
Available online 16 May 2019

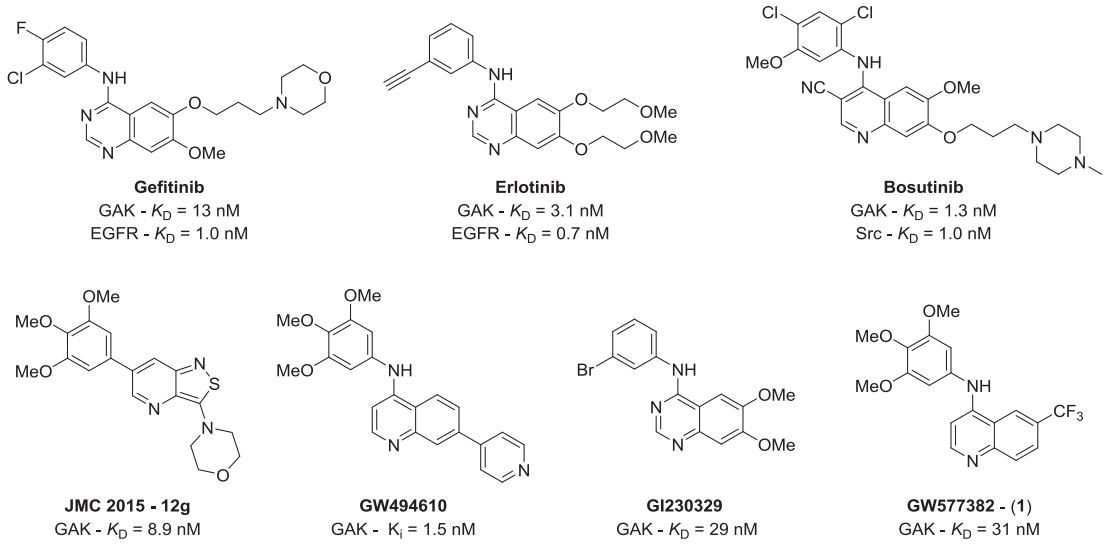

Figure 1. Previously described inhibitors of GAK.

for those kinases with > 60% binding at 1 μM identified three kinases (receptor-interacting protein kinase 2, RIPK2; AarF domain containing kinase 3, ADCK3; and nemo-like kinase, NLK) with K_D values within 30-fold of that of GAK consistent with previous reports.[20,21]

The optimisation of **1** using 4-anilinoquinolines and found that the 3,4,5-trimethoxy aniline was the preferred substitution on the 'head group' of the molecule.[20,21] This head group favourably balanced steric, electronic, and solvent effects. We now report a mini-panel kinome optimisation of quinoline substitution using an enzymatic assay complementary to the GAK binding assays that generated the K_D values (Table 1).

We prepared a series of compounds (**1–22**) through nucleophilic aromatic displacement of commercially available 4-chloroquin(az)olines in excellent yields (58–85%), consistent with previous reports (Scheme 1).[20–23]

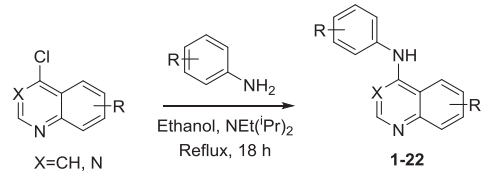

Scheme 1. General synthetic procedure.

Table 1
Affinity of 4-anilinoquinolines for GAK and corresponding mini-kinome panel profile

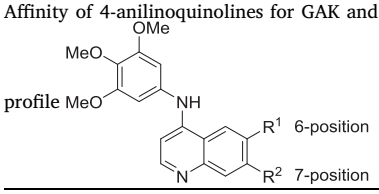

Cmpd	R^1	R^2	GAK	Kinases[b]	
			K_D (nM)[a]	> 70%	> 50%
1	CF_3	H	10	3	7
2	H	H	170	1	2
3	F	H	58	2	2
4	Cl	H	6.3	2	4
5	Br	H	4.1	3	8
6	I	H	8.6	2	7
7	H	F	76	2	2
8	H	Cl	13	5	9
9	H	Br	8.6	10	11
10	H	I	7.6	10	11
11	*t*-Bu	H	34	2	3
12	CN	H	4.9	2	3
13	SO_2Me	H	450	2	4
14	OMe	H	48	1	2
15	OMe	OMe	11	6	9
16	H	OMe	35	1	2
17	H	CF_3	23	5	9
18	H	CN	43	7	12

[a] Eurofins DiscoverX binding assay (n = 2),
[b] Kinases inhibited in enzyme assays at 1 μM – custom panel of 69 kinases (n = 1). (See Fig. S2)

The unsubstituted quinoline (**2**) showed a > 15-fold reduction in potency relative to the 6-CF_3 analog **1**. The 6-position halogen-containing compounds **3–6** showed preference over those with halogens at the 7-position (**7–10**). However, the iodo analogs **6** and **10** do not follow the general trend seen with the other halogens. The larger 6-*tert*-butyl (**11**) was 3-fold weaker than **1**, and 6-cyano (**12**) showing a doubling of potency. The 6-methylsulfone (**13**) was considerably weaker with > 2 orders of magnitude loss in binding potency. The methoxy isomers (**14–16**) did not yield increased potency relative to the halogens, but **15** showed that the substitution pattern does affect GAK potency with a 3–5-fold improvement over mono-substituted analogs **14** and **16**. The 7-position trifluoromethyl (**17**) and cyano (**18**) showed no improvement over the corresponding 6-position counterparts **12** and **1** respectively

We employed a custom panel of sixty-nine kinase activity assays to measure kinome-wide selectivity at 1 μM compound (Table 1, Table S1, Fig. 2). This panel included all off-targets of

1 as well as a standard panel of diverse kinases from different branches of the kinome phylogenetic tree. On the quinoline core, 7-position halogens (**8–10**) in addition to 7-trifluoromethyl (**17**) and 7-cyano (**18**) showed affinity for ABL. The same trend was observed with ALK2 with increased potency (80–90% inhibition) and to a lesser extent with ALK6. c-RAF was also potently inhibited across the series, with inhibition range of 70–90 %. However, the monomethoxy compound **16** showed reduced activity by 20% on c-RAF showing that selectivity could be achieved. EGFR showed no significant activity at 1 μM across the series, despite extensive previous reports of EGFR activity on more decorated quin(az)oline structures.[4–5]

The ephrin receptor family showed broadly similar trends with EphA1, EphA8 and Fyn potently inhibited by 7-position halogenated compounds (**8–10**) in addition to 7-trifluoromethyl (**17**) and 7-cyano (**18**). EphA5 and EphB4 showed less sensitivity to changes in substitution but similar trends across the series. Interestingly the 6,7-

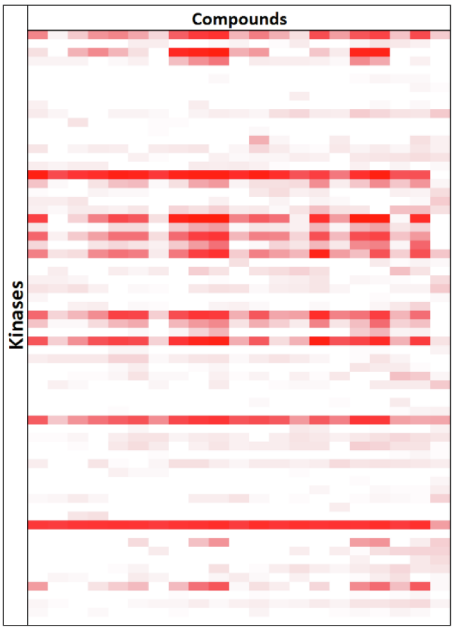

Figure 2. Customized panel heatmap of 69 kinases for 21 quin(az)olines. (Table S1 for details). Screened at 1 μM compound, red is 100% inhibition, white is 0% inhibition relative to DMSO control.

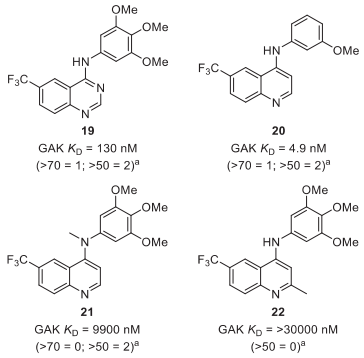

Figure 3. Analogs for further investigation of quinoline pharmacophore. [a]Kinases inhibited Eurofins enzyme assay at 1 μM - Panel of 69 kinases (n = 1).

disubstituted methoxy (**15**) was potent across the whole family as was the *meta*-methoxy 6-trifluoromethyl analog (**20**), suggesting that the structure activity relationship is not solely due to steric effects and is likely influenced by other contributions including electronic and solvation effects (Figs. 2 and 3). Lyn and Lck followed the same trends as the ephrin receptor kinases, suggesting that substitution at the 7-position was increasing promiscuity more generally across the kinome. The last kinase to show sporadic inhibition was Txk with a profile consistent with the previous kinases albeit with reduced sensitivity.

The previously identified off-target nemo-like kinase (NLK) from the original hit compound **1** showed a range of profiles across the series with a pattern similar to the GAK activity. However, the RIPK2 activity was not sensitive to changes in substitution across the compounds tested. This observation held even with some of the more diverse analogs including a quinazoline version of **1** with the possibility of an additional hinge binding interaction (**19**) and a simplified *mono*-methoxy (**20**) but not with the negative controls **21** and **22** (Fig. 3).

Analysis of the active site suggested that GAK Ala47 residue could be exploited to improve selectivity over RIPK2. In comparison to 6-cyano (**12**), the 6-bromo compound (**5**) was expected to have a reduced ability for a direct hydrogen bonding interaction between Ser25 of RIPK2 near the solvent exposed portion of the ATP-binding pocket.[20–22,24] Results from the mini-panel panel structure activity relationships confirmed this supposition, and we chose compounds **5** and **15** for full-kinome follow-up to identify a candidate with the best balance of GAK potency and overall selectivity profile. (Table 2). We had initially screened quinoline **1** to reveal the kinome landscape with over 468 kinases screened, including 402 wild-type human kinases, 63 mutants, and 3 parasite kinases. Only GAK and three other targets (ADCK3, NLK & RIPK2) demonstrated K_D values below 1 μM with **5** further kinases between 1 and 5 μM. We then screened **15**, relating to its potency on target and favourable off-target profile and literature precendence.[20] However we found increased promiscuity across the kinome, particularly for ABL1, EphA6 and RIPK2 with the nearest off-target dropping from a 30-fold window to GAK in **1** to less than a 10-fold window for **15**. This was compounded by the wider range of thirteen off-targets compared to seven for **1** in the 0.1–5 μM range. We then screened compound **5** based on the mini-panel, which showed a narrow kinome profile and a corresponding potent GAK activity. We found the kinome selectivity profile had improved over **1** with increased potency on target. The corresponding negative control (**21**) only bound a single kinase, IRAK3, under 5 μM across the entire assay panel. The kinome profiles of **1**, **15** and **5** show a progression to a compound that is both narrow spectrum and potent on target (Fig. 4). The mini-panels enable an optimsation strategy driven by kinome selectively concurrent with kinase specific potency.

Table 2
Selected kinase profile of 4 key compounds.

Kinase	1	15	5	21
	K_D (nM)[a]			
GAK	10	11	4.1	9900
ABL1-non-Phos.	1900	170	1200	–
ABL1-Phos.	–	92	–	–
ACVR1	–	1300	1000	–
ADCK3	300	250	260	–
BMPR1B	–	280	–	–
EphA1	3100	1300	–	–
EphA8	1100	560	–	–
EphB6	1600	130	710	–
IRAK3	–	–	–	480
LCK	1100	350	–	–
MEK5	–	430	–	–
NLK	690	410	520	–
RIPK2	890	190	110	–
TXK	1400	–	–	–

[a] Binding assay data (n = 1–2), '-' denotes $K_D \geq 10$ μM (See Figure S2 and Table S2 (full results))

We then screened the most promising compounds in a cellular target engagement system.[25,26] The compounds showed in cell engagement of GAK and good concordance with the in vitro binding (Table 3). The starting point **1** already had submicromolar activity (IC_{50} = 210 nM), with the final compound **5** showing similar potency. Compound **15** showed a > 4-fold improvement over **5** but with a mild increase in cross activity with additional kinases. Interestingly the *meta*-methoxy 6-trifluoromethyl analog **20** showed only a modest decrease in cellular potency, with a corresponding increase in ligand efficiency. The negative controls **21** and **22** performed as expected, with the strategically positioned additional methyl groups disrupting binding.

4-Anilinoquinolines and quinazolines are common structural templates for kinase inhibitors, including several approved medicines, with many more under clinical investigation.[4,5] We had previously identified a series of 4-anilinoquinolines as narrow spectrum inhibitors of GAK and now show how we used mini-kinase panels to define several activity wells on different kinases within a focused array of compounds.

The use of the full kinase panel, while ideal, can be both time and cost constrained during short medicinal chemistry cycles. The use of a focused mini-kinase panel is amenable to support early stage compound

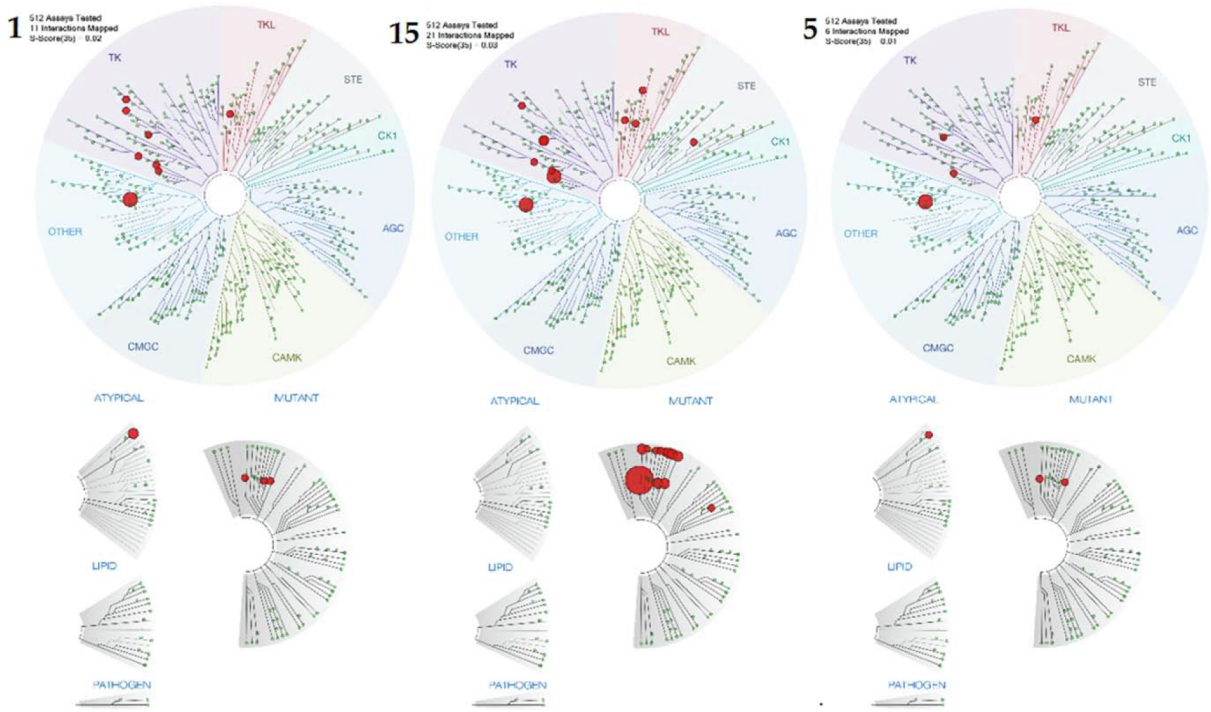

Figure 4. Kinome profiles of 1, 15 and 5 visualization in TREE*spot*.

Table 3
Cellular target engagement profile of key compounds

Cmpd	GAK (nM)[a]	In-Cell (nM)[b]	Kinome[c]
1	10	210	3
5	4.1	200	4
15	11	45	10
19	130	6700	–
20	4.9	380	–
21	9900	> 10000	1
22	> 30000	> 10000	–

[a] Binding assay K_D (n = 2)
[b] Cellular assay IC_{50} (n = 1–2) [c]*scan*MAX kinase hits under 1 μM (excluding GAK) (see Fig. S3).

progression. This early evaluation of selectivity profiles allows for the identification and removal of promiscuous compounds at an early phase of lead optimization, enabling compounds with a narrow kinome profile to progress for lead optimization. This approach also highlights the off-target structure activity relationships enabling them to be designed in or out.

We were able to see clear trends in the mini-panel results in tandem with the scanMAX results. We observed trackable off-targets in the mini-panel including ABL; c-RAF; NLK and RIPK2, but also more sporadic results within the ephrin receptor family (EphA1, A8) and other kinases including ALK2, Lck, Lyn and Txk. There were also clear trends within compound substitutions despite the solvent exposure of this region, with the 7-position showing more promiscuity than the 6-position except for **15**. There were also several one-off weaker hits. These included the 7-cyano (**13**) on CDK9 but no other CDKs. Interestingly, the quinazolines senexin A and B were previously identified as narrow spectrum CDK inhibitors.[27] The switch from the quinoline (**1**) to quinazoline (**19**) saw a slight increase in EGFR activity; further evidence of a complex interplay of structure activity relationships in kinase inhibitor design.

This work highlights the subtleties in kinase inhibitor design where small changes can have a large impact on the kinome selectivity profile. This study illustrates that a carefully crafted, fit for purpose combination of full- and mini-kinome panels can enable efficient discovery of potent and selective inhibitors.

Acknowledgments

The SGC is a registered charity (number 1097737) that receives funds from AbbVie, Bayer Pharma AG, Boehringer Ingelheim, Canada Foundation for Innovation, Eshelman Institute for Innovation, Genome Canada, Innovative Medicines Initiative (EU/EFPIA) [ULTRA-DD grant no. 115766], Janssen, Merck KGaA Darmstadt Germany, MSD, Novartis Pharma AG, Ontario Ministry of Economic Development and Innovation, Pfizer, São Paulo Research Foundation-FAPESP, Takeda, and Wellcome [106169/ZZ14/Z]. We also thank Dr. Brandie Ehrmann for LC-MS/HRMS support provided by the Mass Spectrometry Core Laboratory at the University of North Carolina at Chapel Hill and Caleb Hopkins and Alex Lun for technical support.

Appendix A. Supplementary data

Supplementary data to this article can be found online at https://doi.org/10.1016/j.bmcl.2019.05.025.

References

1. Karaman MW, Herrgard S, Treiber DK, et al. *Nat Biotechnol.* 2008;26:127–132.
2. Bembenek SD, Hirst G, Mirzadegan T. *J Chem Inf Model.* 2018;58:1434–1440.
3. Brandt P, Jensen AJ, Nilsson J. *Bioorg Med Chem Lett.* 2009;19:5861–5863.
4. M.A. Fabian, W.H. Biggs 3rd, D.K. Treiber, et al., Nat Biotechnol 2005;23:329–336.
5. Klaeger S, Heinzlmeir S, Wilhelm M, et al. *Science.* 2017;358:6367.
6. Kovackova S, Chang L, Bekerman E, et al. *J Med Chem.* 2015;58:3393–3410.
7. Kanaoka Y, Kimura SH, Okazaki I, Ikeda M, Nojima H. *FEBS Lett.* 1997;402:73–80.
8. Kimura SH, Tsuruga H, Yabuta N, Endo Y, Nojima H. *Genomics.* 1997;44:179–187.
9. Sato J, Shimizu H, Kasama T, Yabuta N, Nojima H. *Genes Cells.* 2009;14:627–641.
10. Dzamko N, Zhou J, Huang Y, Halliday GM. *Front Mol Neurosci.* 2014;7:57.
11. Zhang CX, Engqvist-Goldstein AE, Carreno S, Owen DJ, Smythe E, Drubin DG. *Traffic.* 2005;6:1103–1113.
12. Eisenberg E, Greene LE. *Traffic.* 2007;8:640–646.
13. Chaikuad A, Keates T, Vincke C, et al. *Biochem J.* 2014;459:59–69.
14. Susa M, Choy E, Liu X, et al. *Mol Cancer Ther.* 2010;9:3342–3350.
15. Sakurai MA, Ozaki Y, Okuzaki D, et al. *PLoS ONE.* 2014;9:e100124.
16. Ray MR, Wafa LA, Cheng H, et al. *Int J Cancer.* 2006;118:1108–1119.

17. Tabara H, Naito Y, Ito A, et al. *PLoS ONE.* 2011;6:e26034.
18. Knapp S, Arruda P, Blagg J, et al. *Nat Chem Biol.* 2013;9:3–6.
19. Drewry DH, Wells CI, Andrews DM, et al. *PLoS ONE.* 2017;12:e0181585.
20. Asquith CRM, Laitinen T, Bennett JM, et al. *ChemMedChem.* 2018;13:48–66.
21. Asquith CRM, Berger BT, Wan J, et al. *J Med Chem.* 2019;62:2830–2836.
22. Asquith CRM, Naegeli KM, East MP, et al. *J Med Chem.* 2019;62:4772–4778.
23. **General procedure for the synthesis of 4-anilinoquinolines**: 6-Bromo-4-chloroquinoline (1.0 eq.), 3,4,5-trimethoxyaniline (1.1 eq.), and iPr_2NEt (2.5 eq.) were suspended in ethanol (30 mL) and refluxed for 18 h. The crude mixture was purified by flash chromatography using EtOAc:hexane followed by 1-5 % methanol in EtOAc. After solvent removal under reduced pressure, the product was obtained as a free following solid. Compounds **1**-**7** and **11**-**22** were synthesised as previously reported.[20–22] **-7-Chloro-*N*-(3,4,5-trimethoxyphenyl)quinolin-4-amine** (**8**) yellow solid (185 mg, 0.538 mmol, 71 %) MP 308-310 °C; ^{1}H NMR (400 MHz, DMSO-d_6) δ 11.21 (s, 1H), 8.92 (d, J = 9.1 Hz, 1H), 8.48 (d, J = 7.0 Hz, 1H), 8.(d, J = 2.1 Hz, 1H), 7.84 (dd, J = 9.1, 2.1 Hz, 1H), 6.87 (d, J = 7.0 Hz, 1H), 6.83 (s, 2H), 3.80 (s, 6H), 3.72 (s, 3H). ^{13}C NMR (101 MHz, DMSO-d_6) δ 155.0, 153.6 (s, 2C), 143.2, 139.1, 138.2, 136.6, 132.6, 127.2, 126.2, 119.2, 115.8, 103.2 (s, 2C), 100.8, 60.2, 56.2 (s, 2C). HRMS m/z $[M+H]^+$ calcd for $C_{18}H_{18}N_2O_3Cl$: 345.1006, found 345.0996, LC t_R = 3.46 min, > 98% Purity. **7-Bromo-*N*-(3,4,5-trimethoxyphenyl)quinolin-4-amine** (**9**) yellow solid (189 mg, 0.483 mmol, 78 %) Decompose > 250 °C; ^{1}H NMR (400 MHz, DMSO-d_6) δ 11.21 (s, 1H), 8.83 (d, J = 9.1 Hz, 1H), 8.47 (d, J = 7.0 Hz, 1H), 8.37 (d, J = 2.0 Hz, 1H), 7.95 (dd, J = 9.1, 2.0 Hz, 1H), 6.87 (d, J = 7.0 Hz, 1H), 6.83 (s, 2H), 3.80 (s, 6H), 3.72 (s, 3H). ^{13}C NMR (101 MHz, DMSO-d_6) δ 155.1, 153.6 (s, 2C), 143.0, 139.1, 136.6, 132.6, 129.8, 127.2, 126.0, 122.3, 116.0, 103.2 (s, 2C), 100.8, 60.2, 56.2 (s, 2C). HRMS m/z $[M+H]^+$ calcd for $C_{18}H_{18}N_2O_3Br$: 389.0501, found 389.0494, LC t_R = 3.53 min, > 98% Purity. **7-Iodo-*N*-(3,4,5-trimethoxyphenyl)quinolin-4-amine** (**10**) yellow solid (176 mg, 0.404 mmol, 78 %) MP 308-310 °C; ^{1}H NMR (400 MHz, DMSO-d_6) δ 11.12 (s, 1H), 8.60 (d, J = 9.0 Hz, 1H), 8.53 (d, J = 1.7 Hz, 1H), 8.44 (d, J = 7.0 Hz, 1H), 8.08 (dd, J = 8.9, 1.7 Hz, 1H), 6.87 (d, J = 7.0 Hz, 1H), 6.82 (s, 2H), 3.80 (s, 6H), 3.72 (s, 3H). ^{13}C NMR (101 MHz, DMSO-d_6) δ 155.2, 153.6 (s, 2C), 142.7, 138.9, 136.6, 135.2, 132.6, 128.4, 125.2, 116.2, 103.2 (s, 2C), 102.0, 100.6, 60.2, 56.2 (s, 2C). HRMS m/z $[M+H]^+$ calcd for $C_{18}H_{18}N_2O_3I$: 437.0362, found 437.0346, LC t_R = 3.70 min, > 98% Purity.

24. Haile PA, Votta BJ, Marquis RW, et al. *J Med Chem.* 2016;59:4867–4880.
25. Kinase binding assays, Kinase enzyme assays KINOMEscan assays and scanMAX assays: preformed as previously described. All assays were provided by Eurofins-DiscoverX (see SI).[1] InCELL Pulse cellular target engagement assays were designed and performed according to manufacturer's instructions (Eurofins-DiscoverX, Fremont, CA. Cat. No. 94-40075).[25].

26. Davies SP, Reddy H, Caivano M, Cohen P. *Biochem J.* 2000;351:95–105.
27. Porter DC, Farmaki E, Altilia S, et al. *Proc Natl Acad Sci USA.* 2012;109:13799–13804.